ESTIMATING DRY MATTER AND TOTAL SOLUBLE CONTENT IN APPLES USING A COMMERCIAL PORTABLE HYPERSPECTRAL IMAGING SYSTEM

Tomislav Medic[1]

[1] Institute of Geodesy and Photogrammetry, ETH Zurich, Zurich, 8093, Switzerland, tmedic@ethz.ch

KEY WORDS: chemometrics, DMC, total soluble solids, TSC, imagery, partial least squares, PLS.

ABSTRACT:

The quest for rapid, non-destructive, and precise technologies for fruit quality estimation is motivated by the needs across the whole food production chain. One of the emerging technologies fulfilling these requirements is spectral imaging. However, despite documented successes, the technology is yet to become established in commercial applications. The best results reported in the literature rely on fixed, non-portable dedicated setups, and controlled light conditions, which limits the potential use cases along the food production chain. In our study, we investigate the possibility of estimating dry matter content (DMC) and total soluble content (TSC) of store-bought apples in non-regulated indoor conditions using a commercial, portable, hand-held imaging system featuring a hyperspectral camera. The acquired images are transformed into per-fruit representative spectral profiles, pre-processed, and analyzed using partial least squares (PLS), the established method in the chemometrics community. We achieved the R^2 of 0.93 for TSC and 0.91 for DMC on the test dataset, with a mean absolute error of 0.71 °Brix for TSC and 0.7% for DMC, which is comparable to the state-of-the-art results presented in the literature. These results indicate that recent instrumental developments enable the deployment of spectral imaging systems in a wider range of tasks in food production, requiring portability and allowing for less stringent control of environmental conditions.

1. INTRODUCTION

Non-destructively estimating internal fruit quality is critical for different parts of the food production chain. It ensures that fruits are harvested at the optimal time, preventing losses due to over-ripening, it helps producers to monitor the quality during storage and transportation, reducing the risk of fruit deterioration, and it helps consumers to receive produce that meets their expectations. Hence, such practices can help reduce waste, and, therefore, improve sustainability, efficiency, and profitability (Abasi et al., 2018).

Hyperspectral imaging offers several benefits over other established methods for non-destructive fruit quality estimation, such as using the dedicated VIS-NIR handheld and table spectrometers (Goisser et al., 2021). Primarily, the estimation requires no contact with the fruit, it is fast, it can be used to evaluate large quantities, and it provides a higher level of completeness and analysis of heterogeneity (Pathmanaban et al., 2019). The results presented in the literature clearly demonstrate that hyperspectral imaging can detect changes in pigments, moisture content, and sugar levels, which are all key indicators of fruit ripeness and quality heterogeneity (Pathmanaban et al., 2019). However, these results almost exclusively relate to cases of using setups that were bulky, non-portable, specially designed for the purpose, and required chambers with a controlled environment, primarily light conditions (Fan et al., 2016; Ma et al., 2022; X. Tian et al., 2019; Y. Tian et al., 2022).

The recent advancements in hyperspectral imaging technology made it more affordable, accessible, and broadly applicable. The emergence of lower-cost portable systems allowed their integration with mobile mapping platforms and robots allowing for on-site, in-field, and more automatic deployment in a range of remote sensing tasks in agriculture. The literature regularly reports successful use cases of yield and nutrition status estimation, as well as stress detection, primarily relying on spectral analysis of leaves properties (Lu et al., 2020). However, to the best of the author's knowledge, there are no investigations answering whether such portable imaging systems would have adequate data quality to also estimate inner fruit quality with sufficient precision to be readily applicable in the industry. The current industry standard for portable spectroscopy is using handheld point spectrometers (Goisser et al., 2021) requiring direct contact with the fruit (or allowing a few cm distances) and providing single spectral profiles without any information about their spatial relations. Enabling on-site automatic hyperspectral imaging for fruit quality estimation across the whole production chain would allow for high throughput phenotyping, also supporting research efforts by notably increasing processable sample sizes for statistical analyses.

To that end, in this work, we investigate the applicability of such a commercial and portable hyperspectral imaging system for estimating inner fruit quality. We demonstrate our results in the case of estimating total soluble content (TSC) and dry matter content (DMC) of store-bought apples in a standard non-regulated indoor environment. We analyzed several different data processing pipelines commonly encountered in chemometrics to give clear recommendations to the end users. We test for generalizability by fitting the regression model for cases of single and multiple apple varieties. Finally, we investigated if additionally integrating RGB information helps the estimation, as it is an inexpensive data source commonly paired with hyperspectral imaging systems.

This article is structured as follows. A short overview of the relevant state-of-the-art and motivation for the study are given in this section (Section 1). Section 2 presents the experiment setup, and describes used hyperspectral imaging system and data processing workflow; Section 3 presents the main results and related discussion, while the main conclusions are drawn in Section 4.

2. MATERIALS AND METHODS

2.1 Experiment setup

The reference values for TSC and DMC were obtained by established destructive methods, and these values were compared against the estimates based on the apples' spectral profiles acquired using a hyperspectral imaging system. Our setup is based on the common setup for calibrating commercial VIS-NIR handheld spectrometers, see e.g. (Zhang et al., 2019). Overall, we processed 80 apples of 8 different varieties, which were bought in a local supermarket (Table 1). Multiple varieties were used to test for the generalizability of the results. However, one variety had a larger sample size (39 apples, roughly 50%) to test if the estimation accuracy is altered when sample variability is reduced.

VARIETY	F#	S#	μ_{TSC}	σ_{TSC}	μ_{DMC}	σ_{DMC}
Golden	10	30	12.93	1.35	15.05	1.47
Gala	6	18	11.94	0.95	13.83	1.17
Jazz	5	15	13.39	0.85	15.26	0.90
Golden Delicious	39	117	16.24	2.91	18.56	3.24
Green Star	5	15	11.36	0.50	13.21	0.58
Pink Lady	9	27	14.44	1.18	16.74	1.07
Juliet	5	15	13.74	1.54	16.20	1.74
Gravenstein	1	3	12.70	0.26	14.70	0.16
ALL	80	240	14.62	2.79	16.83	3.03

Table 1. Apples information summary: number of processed fruits (F#) and overall samples (S#); per variety mean and standard deviation of reference TSC in °Brix and DMC in %.

The apples were measured with a hyperspectral imaging system at an approximately 0.5-meter distance (indicated as optimal by the instrument), at 3 evenly distributed locations per fruit, marked approximately at their equator (simple dash with a number), and separated approximately by 120°. We captured one hyperspectral and one RGB image per location with the marker approximately aligned with the center of the image. The system was handheld during the data acquisition.

For the destructive reference measurements, which directly followed, we carved out cylindrical samples (2.7 cm in diameter and 2 cm in height) with a borer around the marking signalizing the location of the image center. Each apple sample was first peeled and then split into 2 approximately equal halves.

The first half was used for the estimation of TSC using a dedicated digital handheld pocket refractometer (model PAL-1, ATAGO Co., Ltd., Japan). The apple juice was pressed using an ordinary metal kitchen garlic press and applied on the refractometer for the readings using a plastic pipette. The application and reading were repeated 3 times for each sample to control for eventual erroneous readings. The average (median) value of three measurements was considered as the final value for each sample. The acquired reference values for TSC are expressed in Brix degrees (1 °Brix = 1 g of soluble solids in 100 g of solution) with the instrument's measurement range of 0 to 60 °Brix, accuracy of ± 0.2 °Brix, and resolution of 0.1 °Brix.

The DMC was calculated as the ratio (%) of the dry and wet mass of the second halves of the cylindrical fruit samples. The weight measurements were taken using an analytical balance (KUBEI 996), with a resolution of 0.001 g and an accuracy of 0.003 g. After wet weight measurements the samples were left for drying at 65°C in a fruit dehydrator (Graef model DA506EU) for 24h, after which the dry mass measurements were taken. The approach follows the similar experimental setup described in Kumar et al., (2015).

The experiment was done in our measurement facilities with non-controlled light conditions but with a centrally regulated air conditioning system.

2.2 Hyperspectral imaging sensor

For the hyperspectral imaging, we used HAIP BlackMobile (Figure 1), a portable system adapted for handheld operations by HAIP Solutions GmbH (Hannover, Germany). It covers the spectral range of 500-1000 nm with 100 bands (5 nm width). The spectral range is comparable to the spectrometers dedicated to fruit quality estimation present in the reviewed literature (Goisser et al., 2021) and is, therefore, suitable for sensing TSC and DMC.

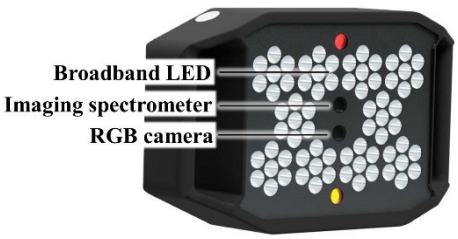

Figure 1. Hyperspectral imaging system, HAIP BlackMobile

The system comprises a push-broom imaging spectrometer, a 4K RGB camera and a broadband LED light source. The hyperspectral images have a resolution of 640 x 480 pixels (22 x 16.5 cm @ 0.5 m) and are captured during the LED light exposure over >3 s period. The instrument was used with default manufacturer settings, including the manufacturer's reflectance calibration using a white reference target as a reflectance standard.

2.3 Data and data processing

The reference values for the TSC and DMC are generated as described in Sec. 2.1, where some observations (less than 1%) were marked as outliers based on the experiment log and removed from further processing. Both values of interest were approximately uniformly distributed ranging from approx. 10-20 °Brix for TSC and 12-24 % for DMC and they were mutually highly correlated (ρ = 98 %), which is a documented phenomenon for apples, as they primarily consist of sugars and water (Travers et al., 2014).

The hyperspectral images (Figure 2) are transformed into single representative (mean) spectral profiles for each of the 3 locations distributed over each fruit (Section 2.1). Approximately centrally located image patches of 50 x 50 pixels (150 x 150 for RGB images due to higher resolution) are separated from the entire image, providing 2500 individual spectral profiles. This size of the patch approximately corresponds to the size of the apple sample acquired for the destructive reference measurements.

In Figure 2 we can observe systematic distortion of the reflectance values due to partially specular reflection from the fruit's surface. We presume that the impact of this phenomenon primarily affects the overall magnitude of the acquired spectra generating an offset that can be successfully mitigated by signal-processing strategies. Therefore, the collected spectral profiles underwent preprocessing using several established strategies (Wang et al., 2015), with the goal of finding the one proving the best TSS and DMC estimation results. We tested: 1) baseline correction by mean subtraction ("Mean"), 2) standard normal variate ("SNV"), 3) calculating 1st and 4) 2nd derivative of the reflectance spectra, 5) vector norm signal normalization ("Vnorm"), 6) transformation of the reflectance R into absorbance A spectra ("Abso") using the simplified relationship A = log (1/R). Besides mitigating eventual distortions in the spectra, this step has the role of feature engineering and has the potential of increasing the sensitivity towards signals of interest.

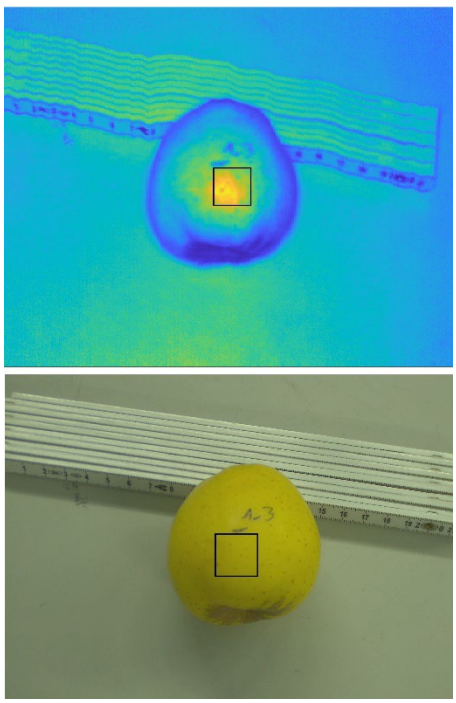

Figure 2. Exemplary hyperspectral (colormap: reflectance at 670 nm wavelength) and RGB image; black rectangles - processed image patches.

The representative spectral signatures for each fruit sample were generated by computing the mean from 2500 samples (pixels). These representative profiles (case: transformation just by subtracting the mean value) are given in Figure 3 for all fruit samples (color according to the reference TSC value; DMC directly comparable). As can be seen in the figure, the representative profiles are smooth due to averaging a high number of individual spectra. Hence, we investigated the impact of signal-smoothing strategies to a limited extent. We only investigated the impact of applying the Savitzky-Golay filter (filter settings based on trial and error: window size = 7, polynomial degree = 3) which is one of the domain standards (Wang et al., 2015).

Several clear features related to TSC can be observed in Figure 3. The most prominent one is the drop of reflectance (increased absorbance) at 670 nm for the fruit samples with low TSC. This phenomenon is related to chlorophyll a concentration in mesocarp and is known to be an important indicator of fruit maturity (Musacchi & Serra, 2018). Further features visibly separating samples with different TSC values can be observed over wider spectral bandwidths in visible and early NIR regions. This initial inspection points out the apparent ability of the imaging system to screen for the values of interest.

Such reflectance spectra as presented in Figure 3 were used as input for the estimation of TSC and DMC (each of them separately), following the signal pre-processing. The estimation was done using Partial Least Squares (PLS) with fine-tuning the number of explanatory (latent) variables based on the L2-norm. The abovementioned features of the spectral profiles exhibit higher bandwidths than the spectral resolution of the used imaging system. This suggests that PLS's inherent ability for dimensionality reduction, by mapping the original datasets into a subset of latent variables, will be well utilized and that a relatively small number of latent variables will be required for the regression.

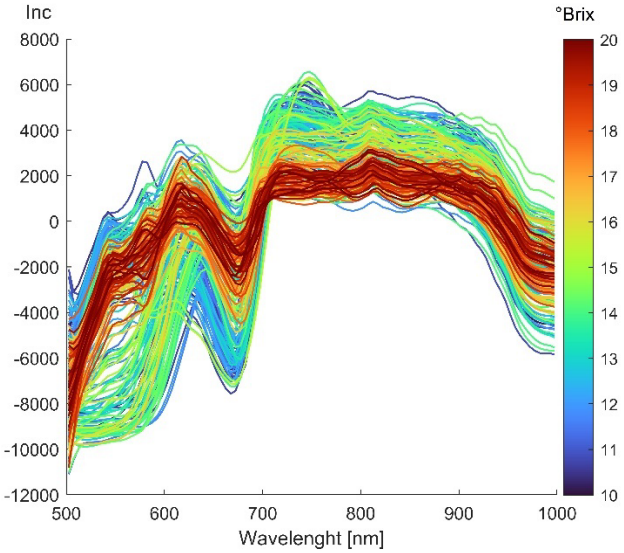

Figure 3. Rainbow plot of all acquired reflectance spectral profiles (average, representative profiles per sample / hyperspectral image) colored according to reference TSC value.

The dataset is split into test and training data using the Kennard-Stone algorithm (Kennard & Stone, 1969) with a 25 to 75 % ratio. We chose PLS due to its attested success in this application domain (standard chemometric tool), as well as to be directly comparable with the results reported in comparable studies. We did not investigate the estimation using potentially more powerful machine learning approaches, such as CNNs despite some evidence that they could outperform the PLS (Mishra & Passos, 2022). This decision was made primarily due to an insufficiently large dataset for training complex regression models. However, we did an investigation of a limited scope, testing some of the common machine learning regression algorithms as alternatives to PLS. The key take-away messages are briefly presented in the following section.

3. RESULTS AND DISCUSSION

Figure 4 presents the best results for estimating TSC and DMC from hyperspectral images of apple samples belonging to 8 different varieties. Expectedly, the results are directly comparable for both values of interest. With the achieved R^2 of 0.8 or more, they demonstrate good generalizability of the regression model across the whole apple species. However, they

fall slightly short of the best results for hyperspectral imaging reported in the literature, which are commonly reporting R^2 in the range of R^2 0.88-0.94 for TSC (Fan et al., 2016; Ma et al., 2022; X. Tian et al., 2019; Y. Tian et al., 2022). However, most of the comparable studies (including all the above-mentioned ones), report the regression results for the models that are calibrated for a single variety of apples.

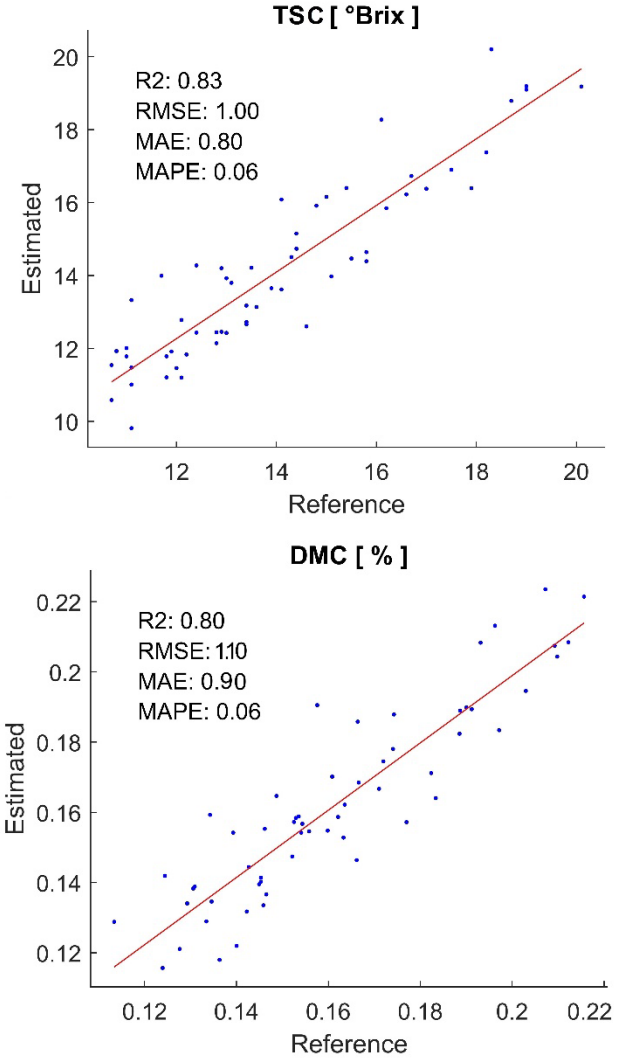

Figure 4. Best estimation results for TSC and DMC: multi-variety case (8 apple varieties, all samples from Table 1).

If our estimation model is calibrated for the single apple variety as well, as in the case presented in Figure 5, the results are further improved reaching state-of-the-art success (R^2 of 0.93 for TSC and 0.91 DMC). Hence, it is apparent that new portable imaging systems, such as the one used in this study, can deliver results of comparable quality, with less stringent setup requirements. From the direct discussion with the industry contacts, we received the information that surpassing R^2 values of 0.90 signals that the technology is deployment ready. Hence, these results also signalize that such portable hyperspectral imaging systems can be readily utilized with standard chemometrics and spectroscopy data processing workflows with satisfactory results.

We expanded our analysis to give a rough impression of the data processing factors that can or cannot influence the estimation results. A brief summary of our observations is presented in the following paragraphs.

Feature (explanatory variables) importance: The optimal number of explanatory latent variables ranged from 10 to 33 for different cases of TSC/DMC estimation and different signal processing strategies. Comparably, the most relevant wavelengths were also case-dependent, and there were no distinctly dominating ones, as PLS projects multiple wavelengths into latent variables. However, generally most dominant clusters can be identified, and they were around peaks at 670 and 730 nm, with further contributing regions around 910, 500-530, and 970-1000 nm. These observations are mostly consistent with the comparable literature relying on VIS-NIR hyperspectral imaging (Fan et al., 2016), besides one discrepancy (500-530 nm band). This confirms that the used portable imaging system has a comparable sensitivity across the spectral range.

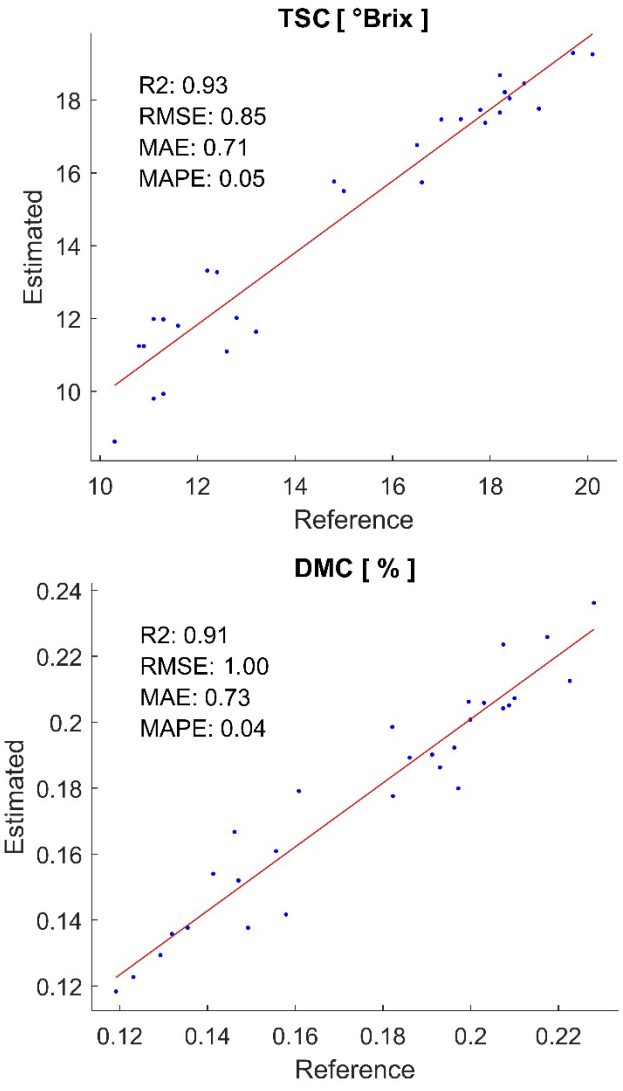

Figure 5. Best estimation results for TSC and DMC: single-variety case (Golden Delicious).

Spectrum smoothing (pre-processing): Applying the Savitzky-Golay filter induced small but consistent improvements of 3-15% in MAE and 1-4% in R^2 value for different signal transformation strategies and TSC and DMC estimation.

Applying other alternative smoothing filters (e.g. moving average window) yielded smaller or negligible improvements.

Spectrum transformation (pre-processing): As can be seen in Table 2, the selection of signal transformation strategy had a small to negligible impact on the overall estimation success. Transforming raw signatures into SNVs and absorbance provided the most consistent benefits. However, the individual best results presented in Figures 4 and 5 were achieved with different strategies. Moreover, in the single-variety case, TSC is the best estimated using the unprocessed reflectance spectra.

		Multi-Variety Case						
		Raw	**Mean**	**SNV**	**1st**	**2nd**	**Vnorm**	**Abs**
TSC	**R^2**	0.77	0.72	0.82	0.75	0.73	0.79	0.83
DMC	**R^2**	0.80	0.75	0.82	0.72	0.75	0.80	0.80
TSC	**MAE**	0.95	1.11	0.82	0.93	0.99	0.87	0.80
DMC	**MAE**	0.90	1.04	0.95	1.04	1.07	0.91	0.90
		Single-Variety Case						
		Raw	**Mean**	**SNV**	**1st**	**2nd**	**Vnorm**	**Abs**
TSC	**R^2**	0.93	0.87	0.90	0.83	0.77	0.82	0.88
DMC	**R^2**	0.88	0.84	0.91	0.83	0.80	0.82	0.87
TSC	**MAE**	0.71	0.82	0.75	0.88	1.15	1.04	0.76
DMC	**MAE**	0.97	0.92	0.73	0.99	1.08	1.08	0.89

Table 2. TSC and DMC estimation results for multi- and single-variety cases using different signal transformation strategies listed in Section 2.3; where Raw corresponds to unprocessed signal and other used abbreviations correspond to the ones given in 2.3. (MAE of TSC is given in °Brix and of DMC in %).

Per-fruit averaging of the spectra: We also investigated if the results can be improved by using one average representative spectra per single fruit instead of per individual sample of the fruit (see Section 2.1 for details). This strategy was notably successful in the single-variety case. The MAE dropped by 43% for DMC and 53% for TSC, while the R^2 increased to 0.98 for both values. Such a strong improvement is probably achieved due to reducing locally present data artifacts and noise both in the reflectance spectra and in the reference values (the noise is not negligible in the latter). Interestingly, in the multi-variety case, such improvements were not observed, and we do not have a plausible hypothesis for this observation.

Inclusion of RGB data: We additionally investigated if including the RGB data can improve the TSC and DMC estimation, as the RGB imagery is automatically captured with the used imaging system. Within this analysis, in the pre-processing step, we applied z-score normalization of features to account for notable scale differences between the pixel values of hyperspectral and RGB images. Additionally, we conducted baseline correction by mean subtraction to RGB images (other pre-processing strategies would be infeasible). The inclusion of RGB values failed to induce any noticeable improvement relative to the best cases presented in Figures 4 and 5. Interestingly, if RGB values alone were used as a predictor of TSC and DMC, in the single-variety case, they achieved R^2 of 0.59 and 0.64 respectively. In the multi-variety case, they were barely better than a random guess achieving R^2 of 0.01 and 0.02 for TSC and DMC respectively.

Alternative regression algorithms: Although we dismissed deep learning as a viable alternative due to limited data size, we conducted a trial of a limited scope using several established machine learning algorithms. Namely, we tested: Lasso (L1-norm on parameters), Random Forest, boosted trees, Gaussian Process regression, and Support Vector Machines (linear). All algorithms were trained with 75-25% train-test split, the L2-norm loss function, with the hyper-parameter tuning of all eligible parameters using k-fold (k = 10) cross-validation using Bayes optimization algorithm over 100 iterations. Lasso regression yielded comparable, or for a few percent worse results relative to the PLSs, while the other algorithms notably underperformed. The most plausible cause for this is that, unlike PLS and Lasso, the remaining algorithms do not have an intrinsic mechanism for coping with a high number of mutually strongly correlated explanatory variables. However, we did not further pursue this analysis through additional variable selection, as it was not the main focus of the study.

4. CONCLUSION

In this work, we demonstrated the successful estimation of dry matter content (DMC) and total soluble content (TSC) of store-bought apples using a commercial and portable hyperspectral camera in a no-light-controlled indoor environment. The achieved results of the R^2 of 0.93 and 0.91 for TSC and DMC respectively, MAE of 0.71°Brix for TSC, and 0.7% for DMC are directly comparable with the state-of-the-art results of dedicated and non-portable imaging setups operating in dark chambers. The implemented workflow is a simple chemometric standard, relying on single per-image representative 1D spectral profiles and the partial least squares (PLS) algorithm. These results suggest that the achieved instrumental development enables the broadening of use cases for hyperspectral imaging towards automated and remote high-throughput phenotyping, potentially relying on mobile mapping platforms and robots. Further work is necessary to investigate if such portable devices are readily applicable for on-tree fruit quality estimation and if the results are significantly degraded by the presence of sun illumination. Additionally, the question of *up to which distances a comparable estimation success is obtainable* remains unanswered. Our future work will focus on investigating the generalizability of these results across different fruits and the possibility of remote estimation of further fruit quality metrics, primarily fruit firmness, and acidity.

ACKNOWLEDGEMENTS

This work was supported by an ETH Zurich Postdoctoral Fellowship.

The author would like to thank Giovanni Broggini and Simon Kollart from Agroscope for their help with the experiment design and for providing their insight into industry demands, and Tobias Kreklow from HAIP Solutions for providing the information about the hyperspectral imaging system.

REFERENCES

Abasi, S., Minaei, S., Jamshidi, B., & Fathi, D. 2018: Dedicated non-destructive devices for food quality measurement: A review. In *Trends in Food Science and Technology* (Vol. 78, pp. 197–205). Elsevier Ltd. https://doi.org/10.1016/j.tifs.2018.05.009

Fan, S., Zhang, B., Li, J., Liu, C., Huang, W., & Tian, X. 2016: Prediction of soluble solids content of apple using the combination of spectra and textural features of hyperspectral reflectance imaging data. *Postharvest Biology and Technology*, *121*, 51–61. https://doi.org/10.1016/j.postharvbio.2016.07.007

Goisser, S., Wittmann, S., & Mempel, H. 2021: Food-scanner applications in the fruit and vegetable sector. *Landtechnik*, *76*(1), 52–67. https://doi.org/10.15150/lt.2021.3264

Kennard, R. W., & Stone, L. A. (1969). Computer aided design of experiments. *Technometrics*, *11*(1), 137–148.

Kumar, S., McGlone, A., Whitworth, C., & Volz, R. 2015: Postharvest performance of apple phenotypes predicted by near-infrared (NIR) spectral analysis. *Postharvest Biology and Technology*, *100*, 16–22. https://doi.org/10.1016/j.postharvbio.2014.09.021

Lu, B., Dao, P. D., Liu, J., He, Y., & Shang, J. 2020: Recent advances of hyperspectral imaging technology and applications in agriculture. In *Remote Sensing* (Vol. 12, Issue 16). MDPI AG. https://doi.org/10.3390/RS12162659

Ma, X., Luo, H., Zhang, F., & Gao, F. 2022: Study on the influence of region of interest on the detection of total sugar content in apple using hyperspectral imaging technology. *Food Science and Technology (Brazil)*, *42*. https://doi.org/10.1590/FST.87922

Mishra, P., & Passos, D. 2022: Multi-output 1-dimensional convolutional neural networks for simultaneous prediction of different traits of fruit based on near-infrared spectroscopy. *Postharvest Biology and Technology*, *183*. https://doi.org/10.1016/j.postharvbio.2021.111741

Musacchi, S., & Serra, S. 2018: Apple fruit quality: Overview on pre-harvest factors. In *Scientia Horticulturae* (Vol. 234, pp. 409–430). Elsevier B.V. https://doi.org/10.1016/j.scienta.2017.12.057

Pathmanaban, P., Gnanavel, B. K., & Anandan, S. S. 2019: Recent application of imaging techniques for fruit quality assessment. In *Trends in Food Science and Technology* (Vol. 94, pp. 32–42). Elsevier Ltd. https://doi.org/10.1016/j.tifs.2019.10.004

Tian, X., Li, J., Wang, Q., Fan, S., Huang, W., & Zhao, C. 2019: A multi-region combined model for non-destructive prediction of soluble solids content in apple, based on brightness grade segmentation of hyperspectral imaging. *Biosystems Engineering*, *183*, 110–120. https://doi.org/10.1016/j.biosystemseng.2019.04.012

Tian, Y., Sun, J., Zhou, X., Yao, K., & Tang, N. 2022: Detection of soluble solid content in apples based on hyperspectral technology combined with deep learning algorithm. *Journal of Food Processing and Preservation*, *46*(4). https://doi.org/10.1111/jfpp.16414

Travers, S., Bertelsen, M. G., & Kucheryavskiy, S. V. 2014: Predicting apple (cv. Elshof) postharvest dry matter and soluble solids content with near infrared spectroscopy. *Journal of the Science of Food and Agriculture*, *94*(5), 955–962. https://doi.org/10.1002/jsfa.6343

Wang, H., Peng, J., Xie, C., Bao, Y., & He, Y. 2015: Fruit quality evaluation using spectroscopy technology: A review. In *Sensors (Switzerland)* (Vol. 15, Issue 5, pp. 11889–11927). MDPI AG. https://doi.org/10.3390/s150511889

Zhang, Y., Nock, J. F., Al Shoffe, Y., & Watkins, C. B. 2019: Non-destructive prediction of soluble solids and dry matter contents in eight apple cultivars using near-infrared spectroscopy. *Postharvest Biology and Technology*, *151*, 111–118. https://doi.org/10.1016/j.postharvbio.2019.01.009